Experimental investigations of micro-scale flow and heat transfer phenomena by using molecular tagging techniques

IOP Publishing Measurement Science and Technology

Meas. Sci. Technol. **21** (2010) 085401 (14pp) doi:10.1088/0957-0233/21/8/085401

Experimental investigations of micro-scale flow and heat transfer phenomena by using molecular tagging techniques

Hui Hu[1], **Zheyan Jin**[1,4], **Daniel Nocera**[2], **Chee Lum**[1,5] **and Manoochehr Koochesfahani**[3]

[1] Department of Aerospace Engineering, Iowa State University, Ames, IA 50011, USA
[2] Department of Chemistry, Massachusetts Institute of Technology, Cambridge, MA 02139, USA
[3] Department of Mechanical Engineering, Michigan State University, East Lansing, MI 48824, USA

E-mail: huhui@iastate.edu, nocera@mit.edu and koochesf@egr.msu.edu

Received 16 January 2010, in final form 24 May 2010
Published 22 June 2010
Online at stacks.iop.org/MST/21/085401

Abstract

Recent progress made in the development of novel molecule-based flow diagnostic techniques, including molecular tagging velocimetry (MTV) and lifetime-based molecular tagging thermometry (MTT), to achieve simultaneous measurements of multiple important flow variables for micro-flows and micro-scale heat transfer studies is reported in this study. The focus of the work described here is the particular class of molecular tagging tracers that relies on phosphorescence. Instead of using tiny particles, especially designed phosphorescent molecules, which can be turned into long-lasting glowing marks upon excitation by photons of appropriate wavelength, are used as tracers for both flow velocity and temperature measurements. A pulsed laser is used to 'tag' the tracer molecules in the regions of interest, and the tagged molecules are imaged at two successive times within the photoluminescence lifetime of the tracer molecules. The measured Lagrangian displacement of the tagged molecules provides the estimate of the fluid velocity. The simultaneous temperature measurement is achieved by taking advantage of the temperature dependence of phosphorescence lifetime, which is estimated from the intensity ratio of the tagged molecules in the acquired two phosphorescence images. The implementation and application of the molecular tagging approach for micro-scale thermal flow studies are demonstrated by two examples. The first example is to conduct simultaneous flow velocity and temperature measurements inside a microchannel to quantify the transient behavior of electroosmotic flow (EOF) to elucidate underlying physics associated with the effects of Joule heating on electrokinematically driven flows. The second example is to examine the time evolution of the unsteady heat transfer and phase changing process inside micro-sized, icing water droplets, which is pertinent to the ice formation and accretion processes as water droplets impinge onto cold wind turbine blades.

Keywords: molecular tagging velocimetry, molecular tagging thermometry, electroosmotic flows, micro-scale heat transfer, icing physics of water droplets, solidification process

(Some figures in this article are in colour only in the electronic version)

1. Introduction

At present, the most commonly used tool for *in situ* imaging of microflows is the micro-particle imaging velocimetry (μ-PIV)

[4] Present address: School of Aerospace Engineering and Mechanics, Tongji University, China.
[5] Present address: BD Medical, Franklin Lakes, NJ 07417, USA.

technique (Santiago *et al* 1998, Meinhart *et al* 1999). μ-PIV is a *particle-based* technique that derives fluid velocity by observing the motion of tiny tracer particles seeded in the flow. Several issues or implications may arise from the fact that μ-PIV does not directly measure fluid motion, but rather infers it from the motion of tracer particles. μ-PIV measurements may become 'intrusive' when the size of tracer particles is comparable with that of the measurement domain for some micro-flow or nano-flow studies. The applications of particle-based flow diagnostic techniques can also be hampered by the potential interaction of tracer particles with walls (Zettner and Yoda 2003, Jin *et al* 2004) or by complications arising from the electrothermal, electrophoretic and dielectrophorectic forces that act on tracer particles but do not originate from working fluids (Devasenathipathy *et al* 2002, Kim and Kihm 2004, Wang *et al* 2005). For example, when μ-PIV is applied to an electroosmotic flow (EOF), the derived velocity is actually the sum of the electrophoretic velocity of the charged tracer particles and the electroosmotic velocity of the bulk neutral fluid. It is usually quite difficult and troublesome, if not impossible, to precisely decouple the electrophoretic velocity and the electroosmotic velocity, especially for cases with significant temperature variations in EOFs due to Joule heating. The implications of using particle-based flow diagnostic techniques would become much more complicated for micro-scale heat transfer studies, where the density of working fluid usually changes with temperature while the density of tracer particles usually does not. Using molecules as flow diagnostic tracers in such applications can significantly mitigate, and perhaps even eliminate, these issues.

Compared to *particle-based* techniques, *molecule-based* methods are much less perturbative, and molecular tracers can be seeded *in situ* with considerably less interruption to fluid flows. Several molecular tagging techniques have been developed for 'in-channel' velocity measurement in microflows (Paul *et al* 1998, Ross *et al* 2001, Sinton and Li 2003a, 2003b, Molho *et al* 2001, Mosier *et al* 2002, Ross and Locascio 2003). The caged-dye imaging technique is one of the most commonly used molecular tagging velocimetry (MTV) techniques for microfluidic studies (Paul *et al* 1998, Ross *et al* 2001, Sinton and Li 2003a, 2003b). Caged dyes are fluorescent dyes that have been made non-fluorescent by binding chemical groups. The tagging step involves removing the 'caging' groups by exposing the caged dye to ultraviolet (UV) light, thus restoring it to its uncaged (fluorescent) state. In a typical caged-dye imaging experiment, a focused, spatially localized UV laser pulse is used to uncage the dye, thereby tagging the regions of interest. The flow velocity can be derived from the motion of the uncaged fluorescent dye. However, it should be noted that all water-soluble caged dyes currently available are electrically charged when uncaged (Ross and Locascio 2003). Therefore, in electrokinetically driven flows, the motion of the 'charged tag' can be monitored directly, but the motion of the neutral working fluid cannot be. The measurement results must be corrected for the electrophoretic motion of the charged dye in order to derive the electroosmotic velocity of the neutral working fluid. In addition, the caged-dye imaging technique may be ineffective for measurements in polymeric microfluidics because the dye can be adsorbed onto the polymeric walls, which can dramatically affect the behavior of microflows. This is especially true for electrokinetically driven flows. Ross and Locascio (2003) reported that the adsorption of the caged dye onto polymeric walls may cause up to 50% measurement error for PDMS microchips. The progressive uncaging release of charged dye molecules can also vary ion concentrations in working fluids, thereby changing the flow physics in electrokinetically driven flows (Xuan *et al* 2004).

Recently, several microscopic thermometry techniques have also been developed for measuring 'in-channel' fluid temperatures in microfluidics. While NMR (Lacey *et al* 2000), Raman spectroscopy (Liu *et al* 1994), on-chip interferometric backscatter detection (Swinney and Bornhop 2002) and thermochromic liquid-crystal (Chaudhari *et al* 1998) techniques are oftentimes used, the most popular procedure is the microscopic laser-induced fluorescence (μ-LIF) technique (Ross *et al* 2001, Guijt *et al* 2003, Erickson *et al* 2003a). μ-LIF involves seeding the working fluid with temperature-sensitive fluorescent dyes (rhodamine B is widely used) and then making fluid temperature measurements by detecting LIF emission via microscopic imaging. A two-color μ-LIF technique has recently been developed to study thermal transport in microfluidic systems in order to minimize the effects of variations in the intensity of illumination source on temperature measurements for better measurement accuracy (Kim *et al* 2003, Natrajan and Christensen 2009). While several experimental studies have been conducted to use the μ-LIF technique with rhodamine B as the temperature-sensitive dye to measure fluid temperature in polymeric microfluidics (Ross *et al* 2001, Erickson *et al* 2003a), Roman *et al* (2005) suggested that the absorption of rhodamine B molecules onto the walls of the polymeric microchannels may cause ambiguities in the quantitative temperature measurements, and can also modify the surface charge density of the polymeric microchannels. It should also be noted that the temperature sensitivity of most commonly used fluorescence dyes is relatively low in general. For example, the temperature sensitivity of rhodamine B, while highest among the fluorescent dyes, is about 2% $^{\circ}C^{-1}$ (Coppeta and Rogers 1998, Hu *et al* 2006), i.e. the fluorescence intensity decreases about 2% for every 1.0 °C increase in temperature. However, for many micro-scale thermal flow studies, the temperature differences in the measurement domain are usually quite small (i.e. only a few degrees Celsius), and it would be technically challenging to achieve accurate measurements of the small temperature differences due to the low temperature sensitivity of the LIF-based thermometry techniques. The overall temperature sensitivity of the LIF-based method can be increased by utilizing a two-color, two-dye, ratiometric approach while taking advantage of two temperature-sensitive fluorescent dyes with *opposite* temperature sensitivities (e.g., Shafii *et al* (2010) report a temperature sensitivity of about 4% $^{\circ}C^{-1}$). Nevertheless, it would be highly desirable to develop novel thermometry techniques that can provide much higher temperature sensitivity compared to that currently

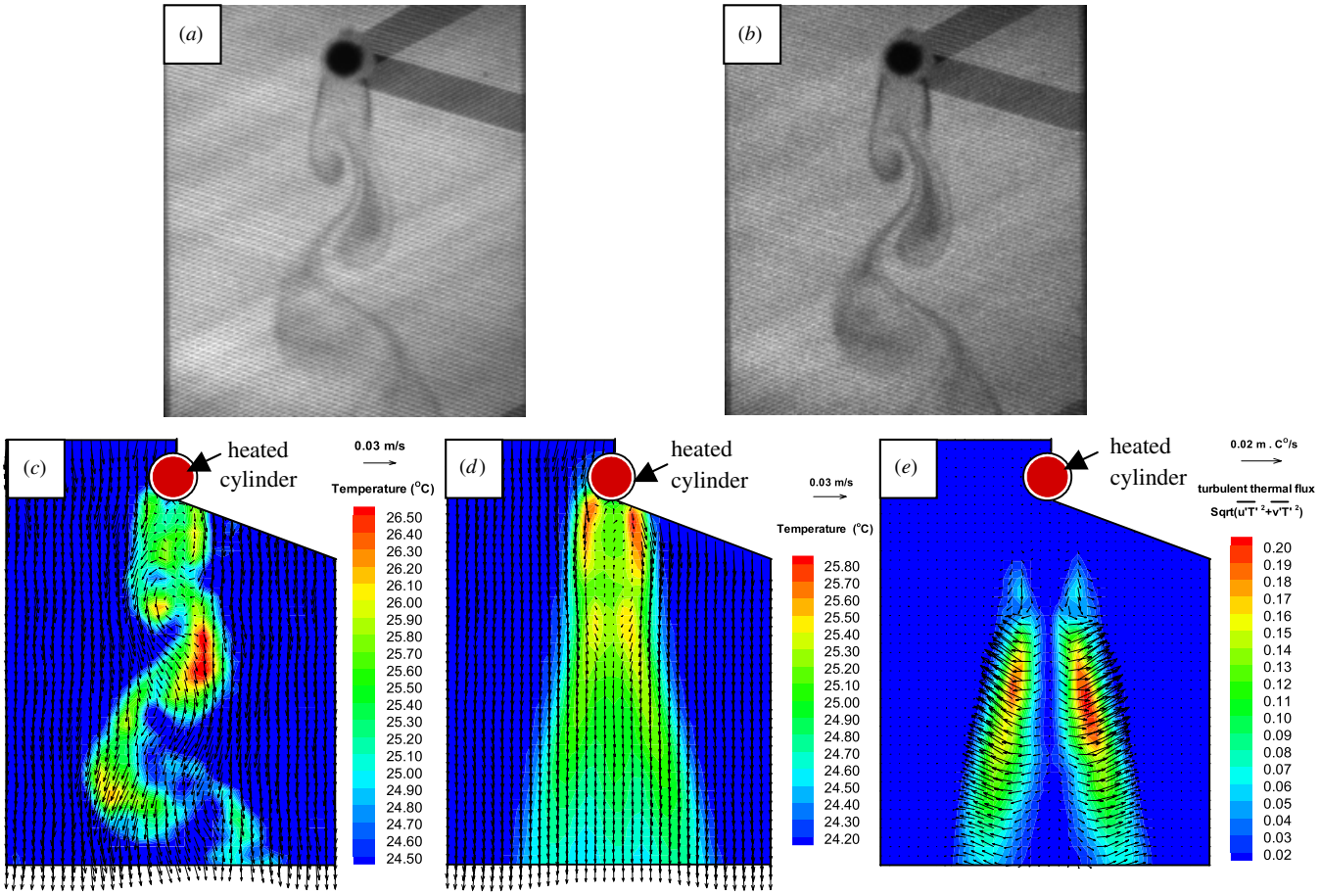

Figure 1. A typical MTV&T image pair and the resultant result: (*a*) grid image at 0.5 ms after the laser excitation pulse; (*b*) 5.0 ms later; (*c*) the simultaneous velocity and temperature fields derived from the images (*a*) and (*b*); (*d*) ensemble-averaged velocity and temperature fields; and (*e*) turbulent thermal flux vectors (Hu and Koochesfahani 2006).

offered by LIF-based thermometry techniques for accurately measuring the small temperature differences for micro-scale heat transfer studies.

It should also be noted that all of the aforementioned microscopic flow diagnostic techniques can measure only either flow velocity or fluid temperature, but not both simultaneously. For many challenging micro-scale thermal fluid problems, such as Joule heating in electrokinetically driven microfluidics, simultaneous determination of flow velocity and fluid temperature is needed in order to elucidate the underlying physics to improve our understanding about the micro-scale thermal flow phenomena. In the present study, we describe the recent progress made in the development of novel *molecule-based* flow diagnostic techniques, including MTV and lifetime-based molecular tagging thermometry (MTT) techniques, for achieving simultaneous measurements of fluid velocity and temperature for micro-flow and micro-scale heat transfer studies.

The work reported here can be considered as the 'microscopic version' of the molecular tagging velocimetry and thermometry (MTV&T) technique developed by Hu and Koochesfahani (2006), which is capable of achieving simultaneous measurements of flow velocity and temperature distributions in 'macro-flows'. Figure 1 shows an example of typical MTV&T measurements. This example is taken from a study of the effect of buoyancy force on the wake instability of a heated cylinder in a water channel (Hu and Koochesfahani 2006). The tracer molecules in the measurement region are tagged by multiple pulsed laser beams in a grid pattern. The figure shows both the initially tagged regions and their subsequent evolution after a time delay of 5.0 ms, together with the resultant simultaneous velocity and temperature distributions derived from the image pair. Because the instantaneous velocity and temperature distributions are measured simultaneously, ensemble-averaged velocity and temperature fields as well as the turbulent thermal flux vectors, i.e. the correlation between the velocity and temperature fluctuations, can be derived from the measurements.

In the following sections, the technical basis of the MTV and lifetime-based MTT techniques will be described briefly along with the related properties of the phosphorescent tracer used for the molecular tagging measurements. The implementation of the molecular tagging techniques for micro-scale thermal flow studies will be demonstrated by conducting simultaneous 'in-channel' velocity and temperature measurements to qunatify the transient behavior of an EOF inside a microchannel to elucidate the underlying physics associated with the effects of Joule heating on

electrokinematically driven flows. In another example, we examine the time evolution of the unsteady heat transfer and phase changing processes within micro-sized, icing water droplets to quantify the important microphysical processes pertinent to wind turbine icing phenomena.

2. Molecular tagging techniques

2.1. Molecular tagging velocimetry

MTV is a 'time-of-flight' method, which can be thought of as the *molecular* counterpart of the particle imaging velocimetry (PIV) for flow velocity field measurements. Compared to PIV, MTV offers advantages in situations in which the use of seed particles is either not desirable or may lead to complications. For MTV measurements based on phosphorescent tracers, especially designed tracer molecules (for the present study, water soluble phosphorescent complex 1-BrNp·Mβ-CD·ROH) are premixed in the working fluid (water, for the present study) and a pulsed laser is used to 'tag' them in the regions of interest. Upon pulsed laser excitation, the tagged tracer molecules emit long-lived phosphorescence, becoming 'glowing' regions that move with the working fluid. Unlike PIV measurements which usually require two pulses of laser illumination for the acquisition of each PIV image pair, in MTV the long-lived phosphorescence emission of the tagged molecules is interrogated at two successive times after the same laser excitation pulse (e.g., a typical pair of the acquired phosphorescence images is shown in figures 1(*a*) and (*b*)). The Lagrangian displacement vectors of the tagged molecules over the prescribed time delay between the two interrogations provide estimates of flow velocity vectors. Various advances in the MTV technique in terms of available molecular tracers, methods of tagging, detection/imaging and data processing can be found in several review articles (Falco and Nocera 1993, Gendrich *et al* 1997, Koochesfahani 1999, Lempert and Harris 2000, Koochesfahani and Nocera 2007), in addition to a special issue of *Measurement Science and Technology* on this topic (Koochesfahani 2000).

In the original work of Gendrich *et al* (1997), for each laser pulse the MTV image pairs were acquired by a pair of aligned image detectors viewing the same region in the flow. In the present study, the two detectors are replaced by a single intensified CCD camera (PCO DiCam-Pro) operating in dual-frame mode, which allows the acquisition of two images of the tagged regions with a programmable time delay between them. The displacement of the tagged regions can be determined by a direct digital spatial correlation technique (Gendrich and Koochesfahani 1996). Similar to the procedure used for PIV image processing, a small window, referred to as the source window, is selected from a tagged region in the earlier image, and it is spatially correlated with a larger roam window in the second image. A well-defined correlation peak occurs at the location corresponding to the displacement of the tagged region by the flow; the displacement peak is located to sub-pixel accuracy using a multi-dimensional polynomial fit (Gendrich and Koochesfahani 1996).

For flow velocity measurement, MTV utilizes only the information about the spatial distribution of the photoluminescence of the tagged molecules within the regions of interest to determine the displacement of the tagged tracer molecules, thereby, the flow velocity. As described in the following section, monitoring the phosphorescence intensity decay rate (i.e. phosphorescence emission lifetime) of the tagged tracer molecules within the tagged regions can provide information of the fluid temperature within those regions simultaneously with flow velocity information.

2.2. Lifetime-based molecular tagging thermometry

It is well known that both *fluorescence* and *phosphorescence* are molecular photoluminescence phenomena. Fluorescence refers to the radiative process when a molecule transitions from a singlet excited state to its singlet ground state. Since singlet–singlet transitions are quantum mechanically allowed, they occur with a high probability, making fluorescence short-lived with emission lifetimes of the order of nanoseconds. Phosphorescence, on the other hand, is a radiative process when a molecule transitions from a triplet excited state to its singlet ground state. Because such transitions are quantum mechanically forbidden, phosphorescence is long lived with emission lifetimes that may approach milliseconds to minutes. Since emission intensity is a function of the temperature for some substances, both *fluorescence* and *phosphorescence* of tracer molecules may be used for temperature measurements. As described above, LIF-based thermometry techniques have been widely used for flow temperature measurements. Recently, *laser-induced phosphorescence* (LIP) techniques have also been suggested to conduct fluid temperature measurements (Thompson and Maynes 2001, Omrane *et al* 2004a, 2004b). Compared to LIF-based thermometry techniques, the relatively long lifetime of LIP could be used to prevent interference from scattered/reflected light and any fluorescence from other substances (such as from solid surfaces) that are present in the measurement area, by simply putting a small time delay between the laser excitation pulse and the starting time for phosphorescence image acquisition. Furthermore, LIP was found to be much more sensitive to temperature variation compared to LIF (Omrane *et al* 2004a, 2004b, Hu *et al* 2006), which is favorable for the accurate measurements of small temperature differences for micro-scale thermal flow studies. The lifetime-based MTT technique described in the present study is a LIP-based method.

According to quantum theory (Pringsheim 1949), the intensity of a first-order photoluminescence process (either fluorescence or phosphorescence) decays exponentially. As described in Hu *et al* (2006), for a dilute solution and unsaturated laser excitation, the collected phosphorescence signal (S) by using a gated imaging detector with integration starting at a delay time t_o after the laser pulse and a gate period of δt can be given by

$$S = AI_i\, C\varepsilon\, \Phi_p(1 - \mathrm{e}^{-\delta t/\tau})\, \mathrm{e}^{-t_o/\tau}, \qquad (1)$$

where A is a parameter representing the detection collection efficiency, I_i is the local incident laser intensity, C is the concentration of the phosphorescent dye (the tagged molecular tracer), ε is the absorption coefficient and Φ_p is the phosphorescence quantum efficiency. The emission

lifetime τ refers to the time at which the intensity drops to 37% (i.e. 1/e) of the initial intensity. For an excited state, the deactivation process may involve both radiative and non-radiactive pathways. The lifetime of the photoluminescence process, τ, is determined by the sum of all the deactivation rates: $\tau^{-1} = k_r + k_{nr}$, where k_r and k_{nr} are the radiative and non-radiative rate constants, respectively. According to photoluminescence kinetics (Ferraudi 1988), these rate constants are, in general, temperature dependent. The temperature dependence of the phosphorescence lifetime is the basis of the present lifetime-based MTT technique.

It should be noted that, in addition to phosphorescence lifetime, τ, resulting in a temperature-dependent phosphorescence signal (S), the absorption coefficient, ε, and quantum yield, Φ_p, are also temperature dependent in general. Thus, in principle, the collected phosphorescence signal (S) may be used to measure fluid temperature if the incident laser intensity and the concentration of the phosphorescent dye remain constant (or are known) in the region of interest. This is the approach taken by Thompson and Maynes (2001), where they quantified the temperature using the phosphorescence intensity acquired with a short fixed time delay (8 μs) after the laser pulse. It should be noted that the collected phosphorescence signal (S) is also the function of incident laser intensity (I_i) and the concentration of the phosphorescent dye (C). Therefore, the spatial and temporal variations of the incident laser intensity and the non-uniformity of the phosphorescent dye (e.g. due to photobleaching caused by continuous incident laser excitations or expulsion of the tracer molecules from the liquid during the icing process) in the region of interest would have to be corrected separately in order to derive quantitative temperature data from the acquired phosphorescence images. In practice, however, it is very difficult, if not impossible, to ensure a non-varying incident laser intensity distribution, especially for unsteady thermal phenomena with a varying index of refraction. This may cause significant error in the temperature measurements. To overcome this problem, Hu and Koochesfahani (2003) developed a lifetime-based thermometry to eliminate the effects of incident laser intensity and concentration of phosphorescent dye on temperature measurements.

The lifetime-based thermometry works as follows. As illustrated in figure 2, laser-induced phosphorescence emission is interrogated at two successive times after the same laser excitation pulse. The first image is detected at the time $t = t_o$ after laser excitation for a gate period δt to accumulate the phosphorescence intensity S_1, while the second image is detected at the time $t = t_o + \Delta t$ for the same gate period to accumulate the phosphorescence intensity S_2. It is easily shown (Hu and Koochesfahani 2006), using equation (1), that the ratio of these two phosphorescence signals (R) is given by

$$R = S_2/S_1 = \mathrm{e}^{-\Delta t/\tau}. \qquad (2)$$

In other words, the intensity ratio of the two successive phosphorescence images (R) is only a funtion of the phosphorescence lifetime τ, and the time delay Δt between the image pair, which is a controllable parameter. This ratiometric approach eliminates the effects of any temporal and spatial

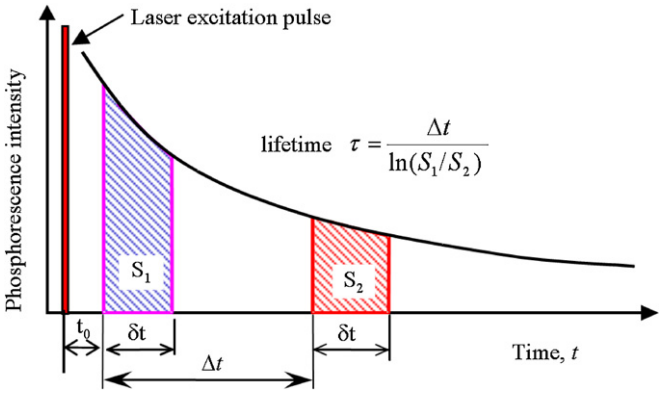

Figure 2. Timing chart of the lifetime-based MTT technique.

variations in the incident laser intensity and non-uniformity of the dye concentration (e.g. due to bleaching or expulsion of the tracer molecules from the liquid water during icing process). For a given molecular tracer and a fixed Δt value, equation (2) defines a unique relation between phosphorescence intensity ratio (R) and fluid temperature T, which can be used for thermometry.

To implement the lifetime-based MTT technique described above, only one laser pulse is required to excite or 'tag' the tracer molecules for each instantaneous temperature field measurement. The two successive acquisitions of the photoluminescence image of the excited or tagged tracer molecules can be achieved using a dual-frame intensified CCD camera. Compared to the two-color LIF thermometry techniques (Kim *et al* 2003, Natrajan and Christensen 2009) which usually require two CCD cameras with proper optical filters to acquire two fluorescent images simultaneously for each instantaneous temperature field measurement, the present lifetime-based MTT technique is easier to implement and can significantly reduce the burden on the instrumentation and experimental setup. Forthermore, since LIF emission is short lived with the emission lifetime on the order of nanoseconds, LIF images are usually acquired when the incident laser illumination is still on; therefore, they are vulnerable to contamination by scattered/reflected light and any fluorescence from other substances. For the lifetime-based MTT technique describe here, as schematically indicated in figure 2, the small time delay between the illumination laser pulse and the phosphorescence image acquisition can effectively eliminate all the effects of scattered/reflected light and any fluorescence from other substances that are present in the measurement region.

2.3. Phosphorescent tracer molecules used in the present study

The phosphorescent molecular tracer used in the present study is the triplex (1-BrNp·Mβ-CD·ROH). The phosphorescent triplex (1-BrNp·Mβ-CD·ROH) is actually the mixture compound of three different chemicals, the lumophore 1-BrNp, maltosyl-β-cyclodextrin (Mβ-CD) and an alcohol (collectively indicated by ROH). Figure 3(a) shows the normalized absorption and emission spectra of the

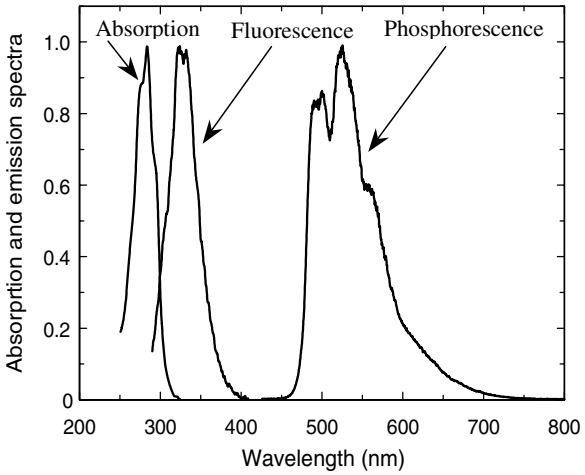

(*a*)

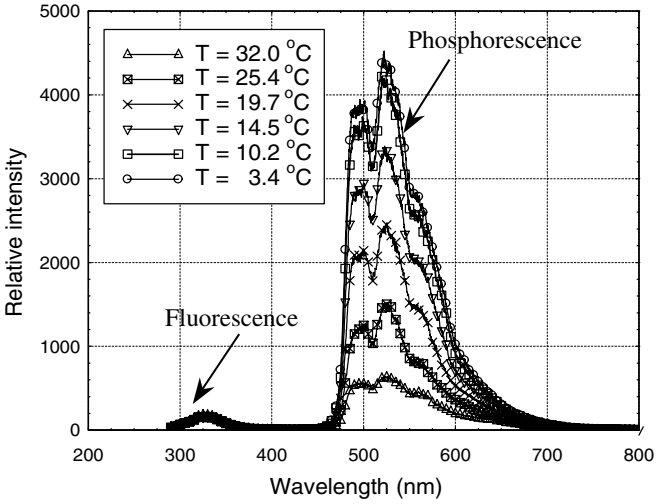

(*b*)

Figure 3. Absorption and emission spectra of the 1-BrNp·Mβ-CD·ROH triplex (Hu *et al* 2006). (*a*) Normalized absorption and emission spectra at room temperature. (*b*) Emission spectra at different temperatures (280 nm excitation of a spectrophotometer).

phosphorescent triplex 1-BrNp·Mβ-CD·ROH. As expected, the phosphorescence emission is significantly red shifted relative to fluorescence. Also note in this figure that, because of the large red shift, there is no overlap between the phosphorescence emission and absorption spectra, and the phosphorescence does not get reabsorbed. Figure 3(*b*) shows the emission spectra at different temperatures. It is clearly seen that the phosphorescence emission of this triplex is very temperature sensitive, whereas its fluorescence is not. The fluorescence lifetime of the triplex was found to be within 20 ns, while the phosphorescence lifetime is much longer, on the order of milliseconds (Hu and Koochesfahani 2003). Further information about the chemical and photoluminescence properties of the phosphorescent triplex is available in Ponce *et al* (1993), Hartmann *et al* (1996) and Koochesfahani and Nocera (2007). In the measurements given in the present study, a concentration of 2×10^{-4} M for Mβ-CD, a saturated (approximately 1×10^{-5} M) solution of

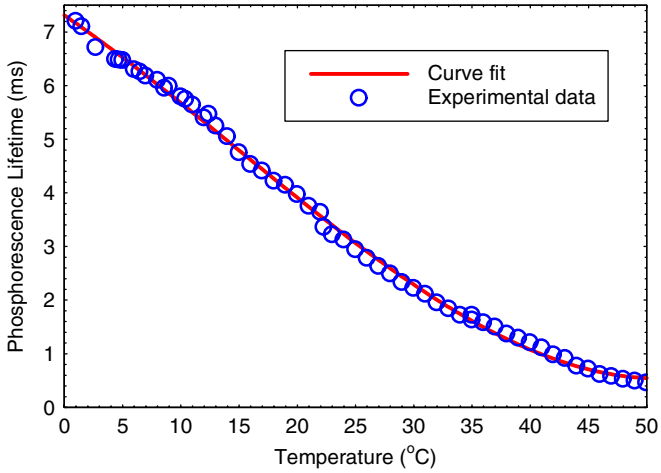

Figure 4. Variation of phosphorescence lifetime versus temperature.

1-BrNp and a concentration of 0.06 M for the alcohol (ROH) were used, as suggested by Gendrich *et al* (1997).

Upon the pulsed excitation of a UV laser (quadrupled wavelength of a Nd:YAG laser at 266 nm for the present study), the phosphorescence lifetime of the phosphorescent triplex (1-BrNp·Mβ-CD·ROH) molecules in an aqueous solution will change significantly with temperature. Figure 4 shows the measured phosphorescence lifetimes of 1-BrNp·Mβ-CD·ROH molecules as a function of temperature, which were obtained though a calibration experiment similar to those described in Hu and Koochesfahani (2006). It can be clearly seen that phosphorescence lifetime decreases from about 7.2 ms to 0.4 ms as the temperature changes from 1.0 °C to 50.0 °C. The relative temperature sensitivity of the phosphorescence lifetime is about 5.0% $^{\circ}C^{-1}$ at 20 °C to 20.0% $^{\circ}C^{-1}$ at 50 °C, which is much higher than those of commonly used fluorescent dyes. For comparison, the temperature sensitivity of rhodamine B for LIF-based thermometry measurements is usually about 2.0% $^{\circ}C^{-1}$ (Coppeta and Rogers 1998, Hu *et al* 2006).

For a given molecular tracer, such as phosphorescent triplex 1-BrNp·Mβ-CD·ROH used in the present study, and fixed Δt value, along with the velocity information of the tagged tracer molecules derived from the MTV measurements described above, equation (2) can be used to calculate the phosphorescence lifetime of the tagged molecules on a pixel-by-pixel basis. It would result in a distribution of the phosphorescence lifetime over a two-dimensional domain. Therefore, with a calibration profile of phosphorescence lifetime versus temperature such as the one shown in figure 4, a two-dimensional temperature distribution can be derived from a phosphorescence image pair acquired after the same excitation laser pulse.

It should be noted, as reported in Coppeta and Rogers (1998), for most commonly used fluorescent dyes in LIF-based thermometry that their fluorescence intensities are pH sensitive. It is usually quite difficult, if not impossible, to decouple the effects of pH and temperature in using LIF-based thermometry techniques for various analytical chemistry and biological applications involving both pH and temperature

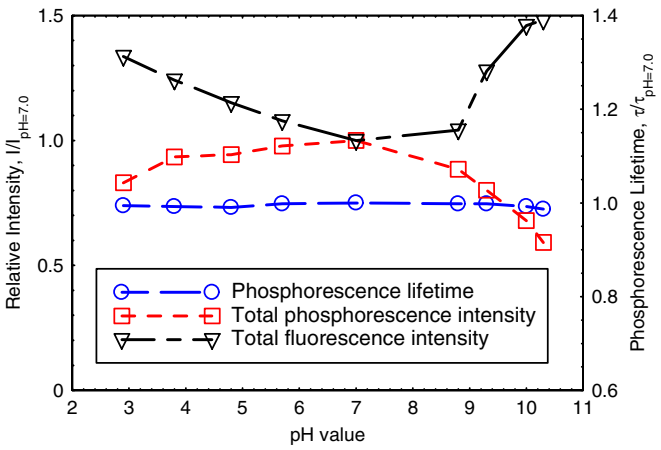

Figure 5. Variations of fluorescence intensity, phosphorescence intensity and phosphorescence lifetime of 1-BrNp·Mβ-CD·ROH molecules versus pH value at the temperature of $T = 20.0\ ^{\circ}$C.

variations within the measurement domain (Murphy *et al* 1985, Thomas and Wimpenny 1996). An experimental study of the effects of pH on the fluorescence and phosphorescence emissions of the phosphorescent triplex 1-BrNp·Mβ-CD·ROH molecules has led to the results shown in figure 5. The total intensities of both fluorescence and phosphorescence emissions of the phosphorescent triplex 1-BrNp·Mβ-CD·ROH molecules were found to be pH sensitive. Interestingly, the phosphorescence lifetime was found to be almost independent of the pH value of the solution (i.e. variations within 1.0%). It suggests that the lifetime-based MTT technique described in the present study can be used as a promising diagnostic tool for various analytical chemistry and biological studies involving both pH and temperature variations in the applications.

An experimental study was also conducted to examine the electrophoretic mobility of the phosphorescent triplex 1-BrNp·Mβ-CD·ROH molecules (Lum *et al* 2004, Lum 2005). It was found that the phosphorescent triplex is neutral in electric charge with no detectable electrophoretic mobility. It suggests that the phosphorescent triplex 1-BrNp·Mβ-CD·ROH can be used as a perfect molecular tracer to conduct quantitative measurements in electrokinetically driven flows. The measured velocity derived from the displacement of this tracer in electrokinetically driven flows represents the pure electroosmotic velocity of the neutral working fluid.

2.4. On the measurement accuracy and resolution of the molecular tagging measurements

The molecular tagging techniques described above, like most measurement techniques, do not give information about fluid flow properties at a 'point'. Rather, they provide the spatially averaged flow velocity and temperature of a molecularly tagged region. Similar to PIV, the effective spatial resolution of the measurement is given by the sum of the source window size and the measured Lagrangian displacement. Clearly, obtaining spatially resolved data for small-scale flow structures would require tagging regions and interrogation windows, consistent with the scales to be resolved. While the best spatial resolution that can be achieved is set by the diffraction limitations of optics used to generate the tagging pattern and the resolution characteristics of image detection, the selection of the source (interrogation) window often involves a choice between the spatial resolution of the measurement and the accuracy of the instantaneous measurement. The temporal resolution of the measurements is set by the time delay Δt between the phosphorescence image pairs. The choice of this time delay influences the accuracy of the velocity data (larger Δt leads to larger Lagrangian displacement of tagged tracer molecules) and the temperature estimation through equation (2). Further discussions about the effects of these factors on the flow velocity and temperature measurement accuracy and spatial resolution by using molecular tagging techniques are avilable in Hu and Koochesfahani (2006), Hu *et al* (2006) and Hu and Huang (2009).

3. Applications of the molecular tagging techniques for micro-scale thermal flow studies

3.1. Qualification of the effects of Joule heating on an electroosmotic flow in a transient state

Fluid transport through microchannels plays a significant role in a great number of emerging technologies such as micro-power generation, chemical separation, cell analysis and biomedical diagnostics (Stone *et al* 2004). A considerable amount of pressure difference may be required to drive a fluid through a channel of tens of micrometers in size by using conventional pressure-driven technology (Li 2004). An alternative and efficient way of moving fluids within microchannels is through electroosmosis, which refers the bulk movement of liquid relative to a stationary charged surface due to externally applied electrical field (Hunter 1992, Probstein 1994). Joule heating is the inherent by-product of the electric work in EOFs. The heat is generated by ohmic resistance of the electrolyte solution due to the passing electrical current. From the microscopic viewpoint, the frequent collision of migrated ions and solvent molecules converts some of the kinetic energy into heat. This scenario is similar to the electrons moving through metal atoms. This internal heat source not only elevates the absolute fluid temperature but also generates temperature gradients in microchannels (Ross *et al* 2001, Guijt *et al* 2003, Erickson *et al* 2003a, 2003b); the flow behavior is therefore strongly affected. The effects of Joule heating can compromise the performance of microfluidics or 'lab-on-a-chip' devices by increasing dispersion in electrokinetic separation and inducing temperature sensitive chemical reactions (Knox and McCormack 1994, de Mello *et al* 2004). Joule heating can also cause local liquid boiling in microfluidics, sometimes even to the point of destroying microchips (Dawoud *et al* 2006). As a consequence, Joule heating and micro-scale heat transfer in electrokinetically driven microfluidics has attracted much attention in recent years.

The inherent nature of the coupling of Joule heating to EOFs requires simultaneous information on electroosmotic velocity and fluid temperature in order to elucidate the

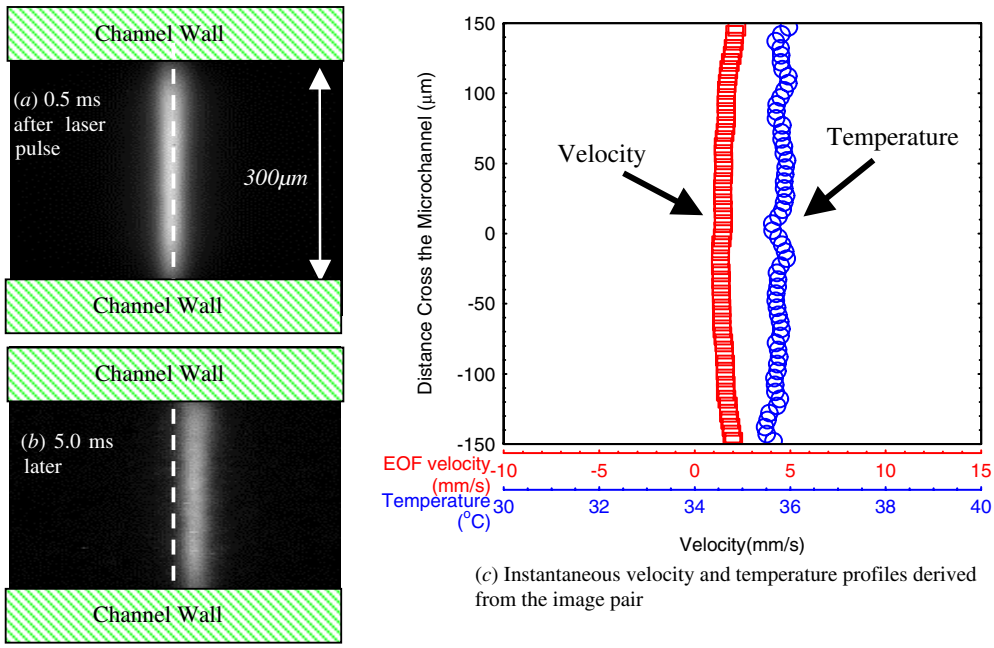

(*c*) Instantaneous velocity and temperature profiles derived from the image pair

Figure 6. A typical molecular tagging measurement in an electrokinetically driven flow (Lum 2005).

underlying physics to further our understanding about Joule heating and the micro-scale heat transfer process in electrokinetically driven microfluidics. As described above, although several flow diagnostic techniques, which include μ-PIV (Wang *et al* 2005), microscopic caged-fluorescent-dye molecular tagging imaging (Sinton and Li 2003a, 2003b, Ross and Locascio 2003), photobleaching molecular tagging imaging (Molho *et al* 2001) and μ-LIF (Ross *et al* 2001, Erickson *et al* 2003a) have been developed for *in situ* measurements in microflows, none of these techniques is capable of achieving simultaneous measurements of 'in-channel' flow velocity and fluid temperature in EOFs.

By using the molecular tagging techniques described above, an experimental study was conducted to achieve simultaneous measurements of EOF velocity and fluid temperature inside a microchannel (Lum *et al* 2004, Lum 2005). In the experimental study, a laser beam from a pulsed Nd:YAG at a quadrupled wavelength of 266 nm was focused to generate a thin laser line of 25 μm in diameter to tag the 1-BrNp·Mβ-CD·ROH tracer molecules premixed with deionized water inside a 300 μm microchannel. A 12-bit gated intensified CCD camera (PCO DiCam-Pro, Cooke Corporation) with a fast decay phosphor (P46) was used to capture the phosphorescence emission. Figure 6 shows an example of the acquired phosphorescence images and the measured 'in-channel' flow velocity and fluid temperature profiles derived from the image pair. The first phosphorescence image was acquired at 0.5 ms after an excitation laser pulse and the second image at 5.5 ms after the same laser pulse with the same exposure time of 1.0 ms for the two image acquisitions. The displacements of the tagged molecular tracers during the time interval between the two image acquisitions can be clearly seen from the comparison of the two phosphorescence images. As described above, since the 1-BrNp·Mβ-CD·ROH tracer molecules are neutral in electric charge (Lum 2005), the displacement of the tagged tracer represents the movement of the neutral working fluid, and the effects of electrophoresis are excluded. While the Lagrangian displacements of the tagged molecules over the prescribed time delay between the two image acquisitions provide the instantaneous EOF velocity profile of the neutral working fluid across the microchannel, the simultaneous fluid temperature measurement is achieved by taking advantage of the temperature dependence of the phosphorescence lifetime of the tagged molecules, which is estimated from the phosphorescence intensity ratio of the tagged molecules in the two acquired images.

It should be noted that most of the previous studies on the Joule heating and EOFs were conducted with the systems already in thermal steady state. Very few investigations are found in the literature to examine the characteristics of EOFs in transient state, where the electroosmotic velocity and temperature change dynamically with time due to the effects of Joule heating. Based on the time sequence of the instantaneous measurement results as those shown in figure 6, the dynamic responses of the electroosmotic velocity and fluid temperature upon the 'switch-on' of an applied electric field can be elucidated quantitatively. The data shown in figure 7 represent the spatially averaged fluid temperature and velocity (i.e. spatially averaged across the channel) inside the microchannel at each instant before and after the 'switch-on' of an electric field of 260 V cm^{-1}. It can be clearly seen that before turning on the applied electric field, the flow velocity is zero and fluid temperature is at room temperature (25.0 °C), as expected. After turning on the applied electric field, due to the effects of Joule heating, the fluid temperature inside the microchannel was found to increase monotonically with time until thermal steady state was reached at about 100 s later. While the applied electric field was kept at a constant value of 260 V cm^{-1}, the EOF velocity inside the microchannel

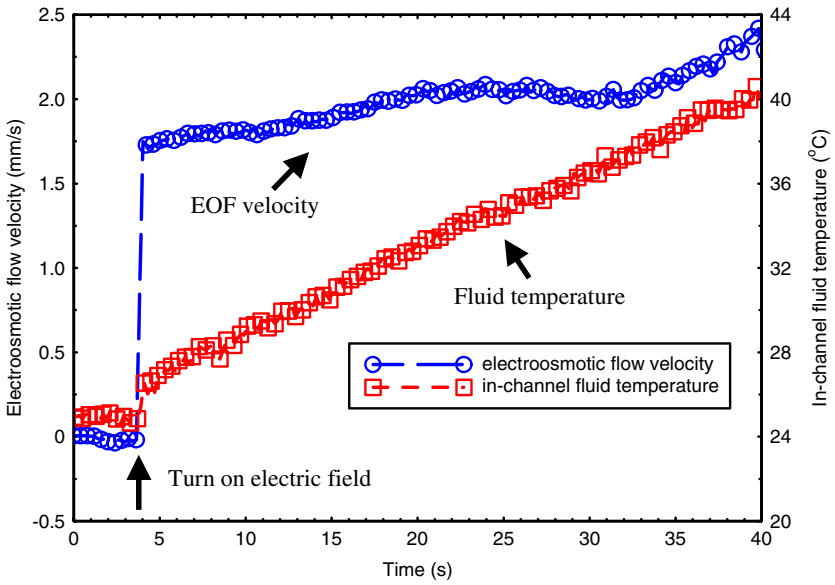

Figure 7. The dynamic response of the 'in-channel' flow velocity and temperature upon turning on of the applied electric field (260 V cm^{-1}) (Lum 2005).

was found to increase slowly with time due to the variations of the fluid viscosity and permittivity associated with the increasing temperature caused by Joule heating (for details see Lum 2005). Based on the simultaneous flow velocity and temperature measurements, as the one presented here, the temperature dependences of fluid permittivity and viscosity can be incorporated quantitatively in examining the effects of Joule heating on EOFs. Further information about the experimental study and the analysis of the measurement results to elucidate underlying physics associated with the effects of Joule heating on EOFs is available in Lum (2005).

3.2. Qualification of the unsteady heat transfer and phase changing process within small icing water droplets pertinent to wind turbine icing phenomena

Wind energy is one of the cleanest renewable power sources in the world today. The US Department of Energy has challenged the nation to produce 20% of its total power from wind by 2030. According to the American Wind Energy Association (AWEA), the majority of wind energy potential available in the USA is in the oceans off the eastern and western seaboards and in the northern states such as North Dakota, Kansas, South Dakota, Montana, Nebraska, Wyoming, Minnesota, and Iowa, where wind turbines are subjected to the problems caused by cold climate conditions. Wind turbine icing represents the most significant threat to the integrity of wind turbines in cold weather. It has been found that ice accretion on turbine blades would decrease power production of the wind turbines significantly (Laakso and Peltola 2005). Ice accretion and irregular shedding during wind turbine operation would lead to load imbalances as well as excessive turbine vibration, often causing the wind turbine to shut off (Dalili *et al* 2009). Icing can also affect the tower structures by increasing stresses. This can lead to structural failures, especially when coupled with strong wind loads (Jasinski *et al* 1998). Icing was also found to affect the reliability of anemometers, thereby, leading to inaccurate wind speed measurements and resulting in resource estimation errors (Homola *et al* 2006). Icing issues can also directly impact personnel safety due to large falling ice chunks (Seifert *et al* 2003).

Due to the lack of knowledge, current ice prediction tools and ice protection system designs for wind turbine applications make use of simple classical models which ignore many details of the important micro-physical processes that are responsible for the ice formation and accretion on wind turbines (Hansman and Turnock 1989, Jasinski *et al* 1998). Advancing the technology for safe and efficient wind turbine operation in atmospheric icing conditions requires a better understanding of the important micro-physical phenomena pertinent to wind turbine icing phenomena. Fundamental icing physics studies capable of providing detailed information to quantify important micro-physical processes such as droplet dynamics, unsteady heat transfer process within water droplets or ice crystals and phase changing process of water droplets and water film flows over smooth/rough surfaces, are highly desirable. While several studies have been carried out recently to simulate ice accretion on turbine blades through icing wind tunnel testing (Hochart *et al* 2008) or using 'artificial' iced profiles with various types and amounts of ice accretion to investigate the aerodynamic performance and power output for iced blades (Tammelin *et al* 1998), very few fundamental studies can be found in the literature to reveal the underlying physics of the important microphysical processes associated with wind turbine icing phenomena.

By using the lifetime-based MTT technique described above, an icing physics study was conducted to elucidate underlying physics to improve our understanding of the important micro-physical processes pertinent to wind turbine icing phenomena (Hu and Jin 2010). Figure 8 shows the schematic of the experimental setup used to quantify the unsteady heat transfer and dynamic phase changing process

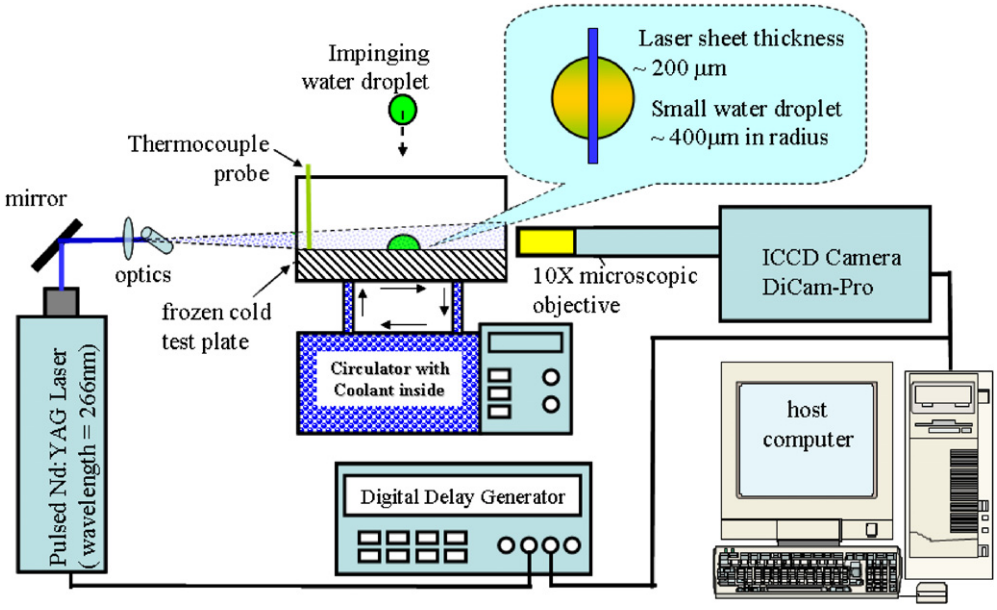

Figure 8. Experimental setup used for the icing physics study.

with small water droplets. A droplet generator was used to generate micro-sized water droplets (about 400 μm in radius and 250 μm in height) to impinge onto a frozen cold test plate to simulate the process of small water droplets impinging onto a cold wind turbine blade. The temperature of the test plate, which was monitored by using a thermocouple, was kept constant at a preselected low temperature level by using a Water Bath Circulator (Neslab RTE-211). The small water droplets would be convectively cooled after they impinged onto the cold test plate. The phase changing process would occur inside the small water droplets when the surface temperature of the test plate was set to below freezing. A set of optical lenses with an adjustable optical slit were used to shape the laser beam from a pulsed Nd:YAG laser (at a quadrupled wavelength of 266 nm) into a laser sheet ($\sim$200 μm in thickness) to tag the premixed 1-BrNp·Mβ-CD·ROH molecules along the middle plane of the small water droplets. A 10$\times$ microscopic objective (Mitsutoyo infinity-corrected, NA = 0.28, depth of field = 3.5 μm) was mounted in the front of an intensified CCD camera (PCO DiCam-Pro, Cooke Corporation) for phosphorescence image acquisition. The camera and the pulsed Nd:YAG laser were connected to a workstation via a digital delay generator (BNC 555 Digital Delay-Pulse Generator), which controlled the timing of the laser illumination and the image acquisition. It is noted that, since low concentration of the phosphorescent triplex 1-BrNp·Mβ-CD·ROH was used for the present study, the effects of the molecular tracers on the physical properties of water are believed to be negligible. During the experiments, the energy level of the pulse laser used to tag the molecular tracers within small water droplets was below 1.0 mJ pulse^{-1}. The repetition rate of the pulsed excitation was 2 Hz. The energy deposited by the excitation laser into the small water droplet was very small, and the temperature rise of the droplets due to the energy deposition of the excitation laser was estimated to be less than 0.1 °C. Further details about the experimental setup and procedures to implement the lifetime-based MTT technique to quantify the unsteady heat transfer and phase changing process within small icing water droplets are given in Jin (2008).

It should be noted that one of the technical challenges to achieve quantitative temperature measurements within icing water droplets is the expulsion of the tracer molecules from the liquid water during the icing process (much like salt is expelled from a saline solution during freezing). This would result in great concentration variations of the tracer molecules in the remaining liquid and cause significant errors in the temperature measurements for commonly used LIF-based thermometry techniques. As described above, since the lifetime-based MTT technique used in the present study is a ratiometric approach, it eliminates the effects of the concentration variations due to the expulsion of phosphorescent tracer molecules during the freezing process.

Figure 9(*a*) shows the time sequence of the acquired phosphorescence images of a water droplet after it impinged onto the frozen cold test plate ($T_W = -2.0$ °C). In the phosphorescence images, the 'brighter' region (i.e. due to more concentrated dye caused by the expulsion of the phosphorescence tracer molecules during icing process) in the upper portion of the droplet represents the liquid phase—water; while the 'darker' region at the bottom indicates the solid phase—ice. It can be clearly seen that the liquid water at the bottom of the droplet was frozen and turned to solid ice rapidly, while the upper portion of the droplet was still in the liquid state. As time goes by, the interface between the liquid phase water and solid phase ice was found to move upward continuously. As a result, the droplet was found to grow upward with more and more liquid phase water turned to solid phase ice. At about 35 s after the droplet impinged onto the cold test plate, the droplet was found to turn into a solid ice crystal completely.

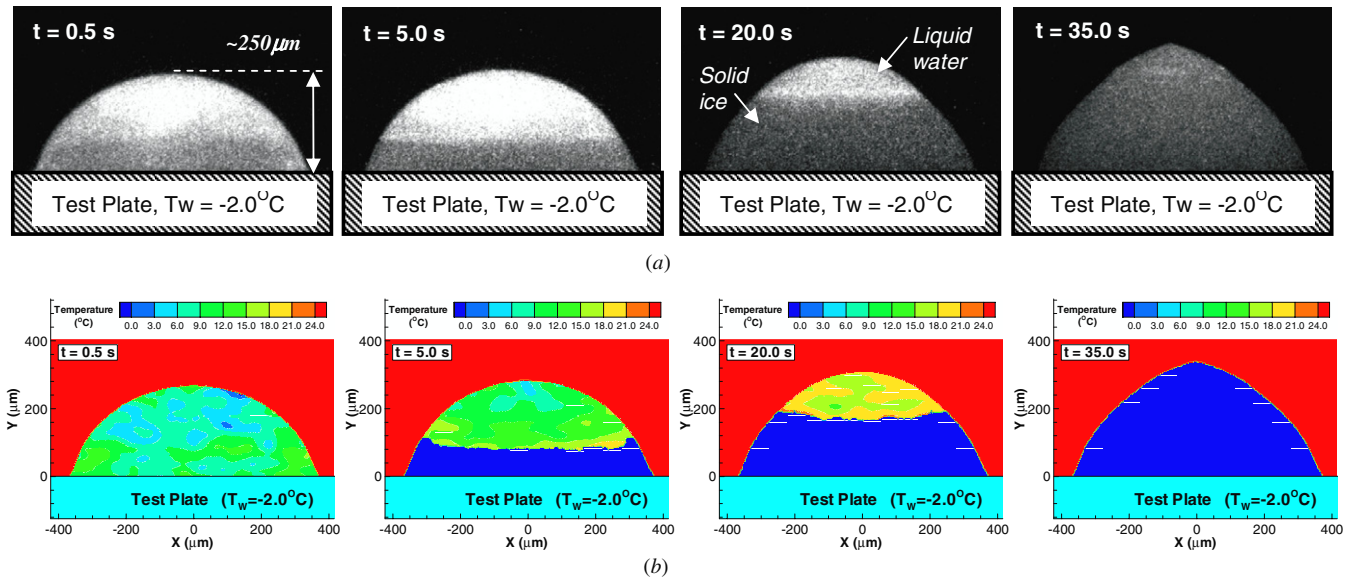

Figure 9. Time evolution of the phase changing process within a small icing water droplet with the surface temperature of the test plate $T_W = -2.0\ ^\circ$C. (*a*) Phosphorescence images. (*b*) Measurement results of the lifetime-based MTT technique.

Figure 9(*b*) shows the corresponding instantaneous temperature distributions of the remaining liquid water within the icing droplet measured by using the lifetime-based MTT technique described above. It should be noted that the MTT measurements were conducted only in the regions where the water droplet exists. The background temperature (i.e. the air temperature surrounding the droplet) shown in the plots was set to a value to best visualize the temperature distribution within the water droplet. As described above, for the MTT measurements shown in figure 9(*b*), the temporal resolution of the measurements was determined by the time interval between the acquisitions of the phosphorescence image pairs, which was 5.0 ms for the present study. Since interrogation windows of 21 × 21 pixels were used for the MTT image processing in the present study, the in-plane spatial resolution of the measurements is about 20 μm × 20 μm. The out-of-plane resolution was estimated to be about 7.0 μm, which is mainly determined by the depth of field of the microscopic objective used for the MTT measurements. The uncertainty of the temperature measurements was estimated to be about $\pm 0.5\ ^\circ$C. Further information about the MTT measurement resolution and uncertainty analysis is available at Hu and Jin (2010).

Based on the time sequences of the instantaneous MTT measurements, as those shown in figure 9(*b*), time evolution of the averaged temperature of the remaining liquid water within the icing droplet in the course of icing process was calculated, which is shown in figure 10. Surprisingly, the averaged temperature of the remaining liquid water within the icing droplet was found to increase monotonically with time in the course of the icing process. The unexpected temperature increase of the remaining liquid water within the droplet in the course of the icing process is believed to be closely related to the heat release of the latent heat of solidification. As a matter of fact, the rapid temperature rise during the freezing of liquid metals caused by the release of latent heat as the

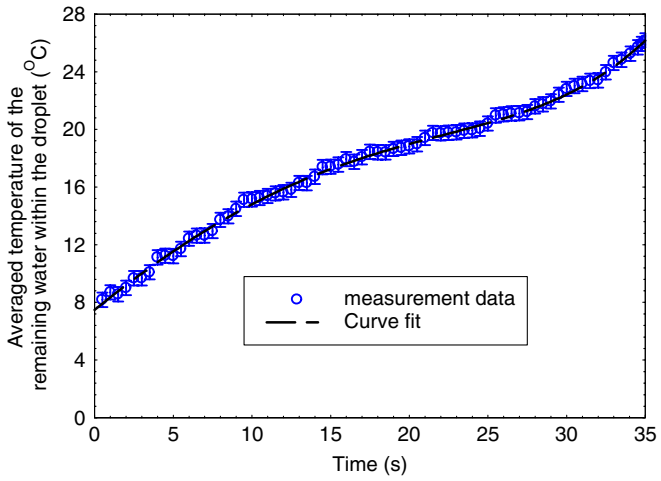

Figure 10. The averaged temperature of the remaining liquid water in the icing droplet versus time when the surface temperature of the test plate was set to $T_W = -2.0\ ^\circ$C.

metals undergo a change in crystalline structure is actually well known in material science and engineering community, which are usually called '*recalescence*' phenomena (Hofmeister *et al* 1990).

Based on the phosphorescent images, the size variation of the icing droplet (in terms of droplet height, contact angle, contact radius, and shape profile) in the course of icing process can also be determined simultaneously. Figure 11 shows the size profiles of the icing droplet extracted from the acquired phosphorescence images. It is well known that a liquid water droplet will experience volume expansion as it turns to solid ice crystal. The time evolution of the droplet volume expansion in the course of the icing process was revealed clearly and quantitatively from the variations of the droplet shape profiles. Interestingly, the height of the droplet was found to increase continuously during the icing process, while the contact radius

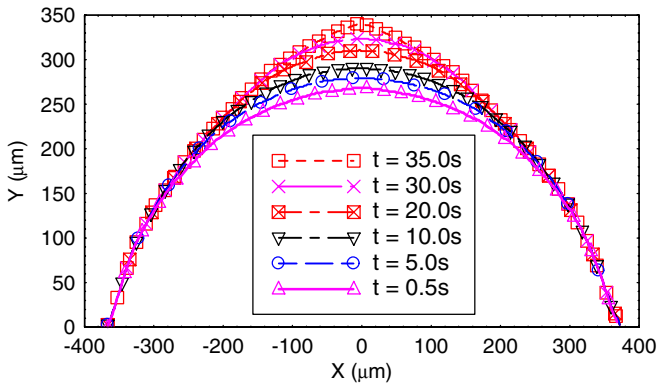

Figure 11. The variations of the the icing droplet shape profile versus time when the surface temperature of the test plate was set to $T_W = -2.0\,^{\circ}\mathrm{C}$.

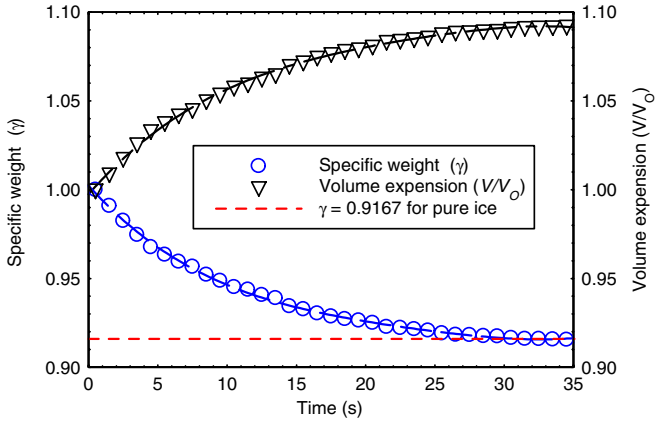

Figure 12. The volume (V/V_O) and the specific weight (γ) of the icing droplet versus time when the surface temperature of the test plate was set to $T_W = -2.0\,^{\circ}\mathrm{C}$.

of the droplet on the test plate was almost constant. It indicates that, in the course of icing process, the volume expansion of the water droplet would be mainly upward to cause droplet growth in height rather than in radius.

The volume of the droplet can be determined quantitatively based on the droplet shape profiles with a reasonable assumption of the droplet being axisymmetric. Figure 12 shows the time evolution of the volume expansion of the droplet, V/V_O, in the course of the icing process, where V_O is the initial volume of the water droplet. It can be clearly seen that the volume of the droplet was found to increase rapidly at the beginning of the icing process since majority of the droplet was still in liquid water state. The volume expansion rate was found to decrease with time since less and less liquid water remained within the droplet. The volume expansion profile was found to become a flat line at about 35 s after the droplet impinged onto the frozen cold test plate, which indicates that the volume of the droplet would not change with time anymore after the water droplet turned to solid ice crystal completely, as expected.

The time variation of the averaged specific weight (thereby, density) of the droplet, γ, in the course of the icing process can also be determined, which is also given in figure 12. For comparison, the standard value of the specific weight of pure ice (i.e. $\gamma_{\mathrm{ice}} = 0.9168$) also indicated in the figure as the dashed straight line. It can be clearly seen that the specific weight (thereby density) of the droplet would become smaller and smaller as more and more remaining liquid water within the droplet turned to solid ice. As expected, the profile of the measured specific weight of the icing droplet was found to approach the standard value of the specific weight of ice (i.e. $\gamma_{\mathrm{ice}} = 0.9168$) as the time goes by. When the water droplet turned into solid ice crystal completely at 35 s after impingement onto the frozen cold test plate, the measured value of the specific weight of the ice crystal was found to be $\gamma = 0.9165$, which agrees with the standard value of specific weight of pure ice $\gamma_{\mathrm{ice}} = 0.9168$ very well.

Based on the measurement results as those shown here, the important microphysical phenomena pertinent to ice formation and accreting process as water droplets impinge onto cold wind turbine blades can be revealed clearly and quantitatively. Such detailed measurements are highly desirable to elucidate underlying icing physics to improve our understanding about the important microphysical processes pertinent to wind turbine icing phenomena. A better understanding of the important micro-physical processes will enable us to improve current icing accretion models for more accurate prediction of ice formation and ice accretion on wind turbine blades and to develop effective and robust anti-/de-icing strategies to ensure safer and more efficient operation of wind turbines in cold weather. Further information about the icing physics experiments and the discussions about the icing physics revealed from the MTT measurements is available in Jin (2008) and Hu and Jin (2010).

4. Conclusions

The present study reported the recent progress made in the development of novel molecule-based flow diagnostic techniques, including MTV and lifetime-based MTT, to achieve simultaneous measurements of multiple important flow variables (such as flow velocity, fluid temperature and droplet size) for microflow and micro-scale heat transfer studies. For the molecular tagging measurements, especially designed tracer molecules are premixed in working fluid. A pulsed laser is used to 'tag' the tracer molecules in the regions of interest. Upon pulsed laser excitation, the tagged tracer molecules emit long-lived phosphorescence and become 'glowing' markers that move with the working fluid. The phosphorescence emission of the tagged molecules is interrogated at two successive times after the same laser excitation pulse. The Lagrangian displacement of the tagged molecules over the prescribed time delay between the two interrogations is used to provide the estimate of flow velocity. The simultaneous temperature measurement is achieved by taking advantage of the temperature dependence of phosphorescence lifetime, which is estimated from the intensity ratio of the tagged molecules in the two acquired phosphorescence images.

In the present study, water-soluble phosphorescent complex 1-BrNp·Mβ-CD·ROH is used as the molecular tracer for the molecular tagging measurements. While

the fluorescence and phosphorescence intensities of the phosphorescent complex 1-BrNp·Mβ-CD·ROH were found to be sensitive to the pH of the solution, its phosphorescence lifetime is almost independent of pH values, which makes it a promising molecular tracer for various analytical chemistry and biological studies involving both pH and temperature variations in the applications. In addition, since the phosphorescent triplex is neutral in electric charge with no detectable electrophoretic mobility, its velocity represents the pure electroosmotic velocity of the neutral working fluid in electrokinetically driven flows.

Two application examples are presented to demonstrate the feasibility and implementation of the molecular tagging techniques to study complex and challenging micro-scale thermal fluid problems. The first example considers simultaneous flow velocity and fluid temperature measurements inside a 300 μm microchannel to qunatify the transient behavior of EOF to elucidate underlying physics associated with the effects of Joule heating on electrokinematically driven flows. The second example is related to applying the lifetime-based MTT technique to achieve simultaneous measurements of droplet size (in terms of volume, height, contact area and the contact angle of the droplet) and temporally-and-spatially-resolved temperature distributions within micro-sized, icing water droplets to quantify the unsteady heat transfer and phase changing process to elucidate underlying physics of the important micro-physical processes pertinent to wind turbine icing phenomena. These examples clearly demonstrate that the molecular tagging techniques can serve as promising tools in the studies of various complex and challenging micro-scale thermal fluid problems to improve our understanding of the important microphysical thermal fluid phenomena.

Acknowledgments

This work was supported by the CRC Program of the National Science Foundation, grant number CHE-0209898, and made use of shared facilities of the MRSEC Program of the National Science Foundation, Award Number DMR-9809688. Additional support by the National Science Foundation CAREER program with award number CTS-0545918 is gratefully acknowledged.

References

Chaudhari A M, Woudenberg T M, Albin M and Goodson K E 1998 Transient liquid crystal thermometry of microfabricated PCR vessel arrays *J. Microelectromech. Syst.* **7** 345–55

Coppeta J and Rogers C 1998 Dual emission laser induced fluorescence for direct planar scalar behavior measurements *Exp. Fluids* **25** 1–15

Dalili N, Edrisy A and Carriveau R 2009 A review of surface engineering issues critical to wind turbine performance *Renew. Sustainable Energy Rev.* **13** 428–38

Dawoud A, Kawaguchi T, Markushin Y, Porter M D and Jankowiak R 2006 Separation of catecholamines and dopamine-derived DNA adduct using a microfluidic device with electrochemical detection *Sensors Actuators* B **120** 42–50

de Mello A J, Habgoodm M, Lancaster N L, Welton T and Wooton R C 2004 Precise temperature control in microfluidic device using joule heating of ionic liquid *Lab Chip* **4** 417–9

Devasenathipathy S, Santiago J G and Takehara K 2002 Particle tracking techniques for electrokinetic microchannel flows *Anal. Chem.* **74** 3704–13

Erickson D, Li D and Krull U J 2003a Dynamic modeling of DNA hybridization kinetics for spatially resolved biochips *Anal. Biochem.* **317** 186–200

Erickson D, Sinton D and Li D 2003b Joule heating and heat transfer in poly(dimethylsiloxane) microfluidic systems *Lab Chip* **3** 141–9

Falco R E and Nocera D G 1993 Quantitative multipoint measurements and visualization of dense solid-liquid flows using laser induced photochemical anemometry (LIPA) *Particulate Two-Phase Flow* ed M C Rocco (London: Butterworth-Heinemann) pp 59–126

Ferraudi G J 1988 *Elements of Inorganic Photochemistry* (New York: Wiley)

Gendrich C P and Koochesfahani M M 1996 A spatial correlation technique for estimating velocity fields using molecular tagging velocimetry (MTV) *Exp. Fluids* **22** 67–77

Gendrich C P, Koochesfahani M M and Nocera D G 1997 Molecular tagging velocimetry and other novel application of a new phosphorescent supramolecule *Exp. Fluids* **23** 361–72

Guijt R M, Dodge A, van Dedem G W K, de Rooij N F and Verpoorte E 2003 Chemical and physical processes for integrated temperature control in microfluidic devices *Lab Chip* **3** 1–4

Hansman R J and Turnock S R 1989 Investigation of surface water behavior during glaze ice accretion *J. Aircr.* **26** 140–7

Hartmann W K, Gray M H B, Ponce A and Nocera D G 1996 Substrate induced phosphorescence from cyclodextrin• lumophore host-guest complex *Inorg. Chim. Acta* **243** 239–48

Hochart C, Fortin G and Perron J 2008 Wind turbine performance under icing conditions *Wind Energy J.* **11** 319–33

Hofmeister W H, Bayuzick R J and Robinson M B 1990 Dual purpose pyrometer for temperature and solidification velocity-measurement *Rev. Sci. Instrum.* **61** 2220–3

Homola M C, Nicklasson P J and Sandsbo P A 2006 Ice sensors for wind turbines *Cold Reg. Sci. Technol.* **46** 125–31

Hu H and Huang D 2009 Simultaneous measurements of droplet size and transient temperature within surface water droplets *AIAA J.* **47** 813–20

Hu H and Jin Z 2010 An icing physics study by using lifetime-based molecular tagging thermometry technique *Int. J. Multiph. Flow* **36** 672–81

Hu H and Koochesfahani M M 2003 A novel technique for quantitative temperature mapping in liquid by measuring the lifetime of laser induced phosphorescence *J. Vis.* **6** 143–53

Hu H and Koochesfahani M M 2006 Molecular tagging velocimetry and thermometry (MTV&T) technique and its application to the wake of a heated circular cylinder *Meas. Sci. Technol.* **17** 1269–81

Hu H, Lum C and Koochesfahani M M 2006 Molecular tagging thermometry with adjustable temperature sensitivity *Exp. Fluids* **40** 753–63

Hunter R J 1992 *Foundations of Colloid Science* (New York: Oxford University Press)

Jasinski W J, Noe S C, Selig M C and Bragg M B 1998 Wind turbine performance under icing conditions *Trans. ASME, J. Sol. Energy Eng.* **120** 60–5

Jin S, Huang P, Park J, Yoo J Y and Breuer K S 2004 Near-wall PTV measurements using evanescent wave illumination *Exp. Fluids* **37** 825–33

Jin Z 2008 Experimental investigations of micro-scale thermal fluid phenomena by using advanced flow diagnostic techniques *PhD Thesis*, Department of Aerospace Engineering, Iowa State University

Jin Z and Hu H 2009 Quantification of unsteady heat transfer and phase changing process inside small icing water droplets *Rev. Sci. Instrum.* **80** 054902
Kim M J and Kihm K D 2004 Microscopic PIV measurements for electro-osmotic flows in PDMS microchannels *J. Vis.* **7** 111–8
Kim H J, Kihm D K and Allen J S 2003 Examination of ratiometric laser induced fluorescence thermometry for microscale spatial measurement resolution *Int. J. Heat Mass Transfer* **46** 3967–74
Knox J H and McCormack K A 1994 Temperature effects in capillary electrophoresis 1: internal capillary temperature and effect upon performance *Chromatographia* **38** 207–14
Koochesfahani M M 1999 Molecular tagging velocimetry (MTV): progress and applications *AIAA Paper*, AIAA-99-3786
Koochesfahani M M 2000 Special Feature: molecular tagging velocimetry *Meas. Sci. Technol.* **11** 1235–300
Koochesfahani M M and Nocera D 2007 Molecular tagging velocimetry *Handbook of Experimental Fluid Dynamics* ed J Foss, C Tropea and A Yarin (Berlin: Springer) chapter 5.4
Laakso T and Peltola E 2005 Review on blade heating technology and future prospects *2005 BOREAS VII Conf. (Saarislkä, Finland, 7–8 March 2005)*
Lacey M E, Webb A G and Sweedler J V 2000 Monitoring temperature changes in capillary electrophoresis with nanoliter-volume NMR thermometry *Anal. Chem.* **72** 4991–8
Lempert W R and Harris S R 2000 Molecular tagging velocimetry *Flow Visualization—Techniques and Examples* ed A J Smits and T T Lim (London: Imperial College Press) pp 73–92
Li D 2004 *Electrokinetics in Microfluidics* (Burlington, MA: Academic Press)
Liu K, Davis K L and Morris M D 1994 Raman spectroscopic measurement of spatial and temporal temperature gradients in operating electrophoresis capillaries *Anal. Chem.* **66** 3744–50
Lum C 2005 An experimental study of pressure- and electroosmotically-driven flows in microchannels with surface modifications *PhD Thesis*, Department of Mechanical Engineering, Michigan State University
Lum C, Hu H and Koochesfahani M M 2004 Simultaneous velocity and temperature measurements in electroosmotically driven flow in a microchannel using molecular tagging velocimetry and thermometry *Proc. 57th Annual Meeting of APS Division of Fluid Dynamics (Seattle, WA, 21–23 November 2004)*
Meinhart C D, Wereley S T and Santiago J G 1999 PIV measurements in a microchannel flow *Exp. Fluids* **27** 414–9
Molho J I, Herr A E, Mosier B P, Santiago J G, Kenny T W, Brennen R A, Gordon G B and Mohammadi B 2001 Optimization of turn geometries for microchip electrophoresis *Anal. Chem.* **73** 1350–60
Mosier B P, Molho J I and Santiago J G 2002 Photobleached-fluorescence imaging of microflows *Exp. Fluids* **33** 545–54
Murphy P A, Hanson D F, Guo Y N and Angster D E 1985 The effects of variations in pH and temperature on the activation of mouse thymocytes by both forms of rabbit interleukin-1 *Yale J. Biol. Med.* **58** 115–23
Natrajan V K and Christensen K T 2009 Two-color laser-induced fluorescent thermometry for microfluidic systems *Meas. Sci. Technol.* **20** 015401
Omrane A, Juhlin G, Ossler F and Alden M 2004a Temperature measurements of single droplets by use of laser-induced phosphorescence *Appl. Opt.* **43** 3523–9
Omrane A, Santesson S, Alden M and Nilsson S 2004b Laser techniques in acoustically levitated micro droplets *Lab Chip* **4** 287–91
Paul P H, Garguilo M G and Rakestraw D J 1998 Imaging of pressure and electrokinetically driven flows through open capillaries *Anal. Chem.* **70** 2459–67
Pringsheim P 1949 *Fluorescence and phosphorescence* (New York: Interscience)
Ponce A, Wong P A, Way J J and Nocera D G 1993 Intense phosphorescence triggered by alcohol upon formation of a cyclodextrin ternary complex *J. Phys. Chem.* **97** 11137–42
Probstein R 1994 *Physicochemical Hydrodynamics: An Introduction* (New York: Wiley)
Roman G T, Hlaus T, Bass K J, Seelhammer T G and Culbertson C T 2005 Sol-gel modified poly(dimethylsiloxane) microfluidic devices with high electroosmotic mobilities and hydrophilic channel wall characteristics *Anal. Chem.* **77** 1414–22
Ross D, Gaitan M and Locascio L E 2001 Temperature measurement in microfluidic systems using a temperature-dependent fluorescent dye *Anal. Chem.* **73** 4117–23
Ross D, Johnson T J and Locascio L E 2001 Imaging of electroosmotic flow in plastic microchannels *Anal. Chem.* **73** 2509–15
Ross D and Locascio L E 2003 Effect of charged fluorescent dye on the electroosmotic mobility in microchannels *Anal. Chem.* **75** 1218–20
Santiago J G, Wereley S T, Meinhart C D, Beebe D J and Adrian R A 1998 A particle image velocimetry system for microfluidics *Exp. Fluids* **25** 316–9
Seifert H, Westerhellweg A and Kröning L 2003 Risk analysis of ice thrown from wind turbines *BOREAS VI Conf. (Pyhä, Finland, April 2003)*
Shafii M B, Lum C L and Koochesfahani M M 2010 In-situ LIF temperature measurements in aqueous ammonium chloride solution during uni-directional solidification *Exp. Fluids* **48** 651–62
Sinton D and Li D 2003a Microfluidic velocimetry with near-wall resolution *Int. J. Therm. Sci.* **42** 847–55
Sinton D and Li D 2003b Electroosmotic velocity profiles in microchannels *Colloids Surf.* A **222** 273–83
Stone H A, Strook A D and Ajdari A 2004 Engineering flows in small devices, microfluidics toward a lab-on-a-chip *Ann. Rev. Fluid Mech.* **36** 381–411
Swinney K and Bornhop D J 2002 Quantification and evaluation of Joule heating in on-chip capillary electrophoresis *Electrophoresis* **23** 613–20
Tammelin B, Cavaliere M, Holttinen H, Morgan C, Seifert H and Santti K 1998 Wind energy production in cold climate (WECO) Project Report 1–38
Thomas L V and Wimpenny J W T 1996 Investigation of the effect of combined variations in temperature, pH, and NaCl concentration on nisin inhibition of *Listeria monocytogenes* and *Staphylococcus aureus Appl. Environ. Microbiol.* **62** 2006–12
Thompson S L and Maynes D 2001 Spatially resolved temperature measurement in a liquid using laser induced phosphorescence *J. Fluid Eng.* **123** 293–302
Wang D, Sigurdson M and Meinhart C D 2005 Experimental analysis of particle and fluid motion in AC electrokinetics *Exp. Fluids* **38** 1–10
Xuan X, Xu B, Sinton D and Li D 2004 Electroosmotic flow with joule heating effects *Lab Chip* **4** 230–6
Zettner C M and Yoda M 2003 Particle velocity field measurements in a near-wall flow using evanescent wave illumination *Exp. Fluids* **34** 115–21